



Journal of Aerospace Technology and Management

ISSN: 1984-9648

ISSN: 2175-9146

Departamento de Ciência e Tecnologia Aeroespacial

Lima, Geraldo Mulato de; Almeida, Robert Cardoso
Fernandes de; Castro, Ruy Morgado de; Alvaro, José Damião
Operational Measurements for Infrared Camera Characterization
Journal of Aerospace Technology and Management,
vol. 9, no. 4, 2017, October-December, pp. 519-528
Departamento de Ciência e Tecnologia Aeroespacial

DOI: <https://doi.org/10.5028/jatm.v9i4.589>

Available in: <https://www.redalyc.org/articulo.oa?id=309457439007>

- How to cite
- Complete issue
- More information about this article
- Journal's webpage in redalyc.org

UDEM redalyc.org

Scientific Information System Redalyc

Network of Scientific Journals from Latin America and the Caribbean, Spain and Portugal

Project academic non-profit, developed under the open access initiative

Operational Measurements for Infrared Camera Characterization

Geraldo Mulato de Lima Filho¹, Robert Cardoso Fernandes de Almeida¹, Ruy Morgado de Castro², Alvaro José Damião²

ABSTRACT: The detection, location, identification and recognition are very important activities for the air forces. Imaging systems are tools used for those functions, so it is mandatory to characterize those systems to really know their actual operational limits. This paper presents a set of measurements for spectral, radiometric and spatial camera characterization to be applied to imaging systems operating in the thermal infrared. A SC5600 camera manufactured by FLIR® Systems was used and assembled with lenses of 27 or 54 mm equivalent focal length. The camera spectral characterization was done by comparison to a calibrated system composed by thermal source, monochromator and a broadband reference detector. The radiometric characterization was performed using an extensive blackbody (CI Systems) for temperatures between 10 and 55 °C to evaluate the camera accuracy and obtain the calibration curves. The spatial characterization was carried out using the same extensive blackbody and 2 standard USAF 1951 machined targets, one made of steel and other of aluminum, serving as masks for the blackbody. Using recycled material, a homemade extended blackbody for outdoor use was built. The results obtained using the 2 blackbodies in laboratory were similar.

KEYWORDS: Infrared, Camera, Calibration, USAF 1951, Blackbody.

INTRODUCTION

An imaging system is generally composed by a collector (usually lenses and/or mirrors), filters, detector, processor, a system for data storage and an output unit. The output can be a monitor that provides an image of the collected electromagnetic radiation. The operational wavelength range of the imaging systems is usually between 0.35 and 15 μm (Lillesand and Kiefer 1994). In addition, every electro-optical system has its unique characteristics and some internal parameters to be settled, which directly implies on the quality of the images to be acquired. This quality may or may not be suitable for target location, identification and/or recognition (Johnson 1958), under certain environmental conditions (atmospheric, altitude etc.) or the scenario in which the target was encompassed (Pace and Sutherland 2001). This paper presents results for a camera with spectral response between 2.5 and 5.1 μm . The measurement procedure can be applied to cameras having different spectral responses, if the respective sources and masks for characterization are available.

The complete characterization of these imaging systems is necessary for knowing the operational limits of the equipment. For example, in the case of using a thermal camera for operational purposes, as search and rescue or maritime patrol, one must previously know: what is the electromagnetic spectrum range at which the camera operates and what is its relative sensitivity (spectral characterization)? What is the accuracy on the electromagnetic radiation measurement (radiometric characterization)? What is the actual field of view of each detector element, or how detailed is the target at a certain distance/altitude (spatial characterization)?

¹.Departamento de Ciência e Tecnologia Aeroespacial – Instituto Tecnológico de Aeronáutica – Programa de Pós-Graduação em Aplicações Operacionais – São José dos Campos/SP – Brazil. ².Departamento de Ciência e Tecnologia Aeroespacial – Instituto de Estudos Avançados – Divisão de Fotônica e Geointeligência – São José dos Campos/SP – Brazil.

Author for correspondence: Alvaro José Damião | Departamento de Ciência e Tecnologia Aeroespacial – Instituto de Estudos Avançados – Divisão de Fotônica e Geointeligência | Trevo Coronel Aviador José Alberto Albano do Amarante, 1 – Putim | CEP: 12.228-001 – São José dos Campos/SP – Brazil.

Received: Dec. 26, 2015 | **Accepted:** Apr. 19, 2017

Once this characterization methodology was applied to a thermal camera, the performance characteristics would be known and this would allow choosing the best camera settings as well as planning the search flight to maximize the mission success.

There are other characteristics to check in an electro-optical sensor (Bower *et al.* 2009), such as: temporal resolution — the range the sensor revisits, more applicable to satellite sensors; noise equivalent power (NEP) — the minimum amount of radiant flux to be received by the sensor, to be equal to the noise of the sensor; noise equivalent irradiance (NEI) — the minimum irradiance to be perceived by the sensor, to be equal to its noise; and the noise equivalent temperature difference (NETD) — the smallest temperature difference that can be measured by the camera. However, at the operational level, the knowledge of the spectral resolution, radiometric resolution and spatial resolution is primary to mission success.

MATERIALS AND METHODS

The characterization of a thermal or visible camera comprises 3 steps: spectral, radiometric and spatial. The camera evaluated in this study was a SC5600 by FLIR® Systems. It is a high-performance thermal imaging camera for industrial and educational use. It has an array of 640×512 pixels, with frequency between 5 and 100 Hz. The detectors are chilled indium antimonide (InSb), with spectral response between 2.5 and $5.1 \mu\text{m}$ (FLIR® Systems 2017). The SC5600 camera used in this study had 2 optical assemblies, one with an equivalent focus of 27 mm and the other, of 54 mm, both by FLIR® Systems. The optical assemblies had an integrated autofocus system.

According to the data sheet, the SC5600 has high sensitivity, precision and speed, keeping an excellent linearity. The smallest observed temperature difference is described as 20 mK (0.020°C). The SC5600 camera can perform temperature measurements from 5 to 300°C , and the integration time can be adjusted by increments of μs .

SPECTRAL RESPONSE

An indirect method was chosen to determine the spectral response. It uses a broadband calibrated detector as reference (Schumaker 1996). The schematic diagram of the experimental arrangement is shown in Fig. 1a and basically includes the following equipment:

- Acton SpectraPro 2500i monochromator — Acton Research Corporation 2003.
- Wide Band Detector Judson Mercury Cadmium Telluride — Judson Technologies LLC 2002.
- Stanford Lock-in Amplifier SR510 — Stanford Research Systems 2013.
- Illuminator IR 6363 Newport® — Newport Corporation 2012.
- Power Supply Newport® 69931 — Oriel Instruments 2002.
- Filters of Edmund Optics® — Edmund Optics 2009.

The results obtained by the Judson detector were used as standard for the camera. Figure 1a shows the schematic diagram and Fig. 1b, the camera assembled for measurements, where: 1 is the camera; 2 is the Judson detector (not assembled); 3 is the monochromator; and 4 is the data acquisition computer. The Judson detector is at the center of Fig. 1b, but it was not assembled for measurement at that moment. Three sets of measurements were registered for the Judson detector and also for the camera: no filter, filter 1 (long pass $4.5 \mu\text{m}$) and filter 2 (long pass $2.5 \mu\text{m}$).

The determination of the spectral response was done in a roundabout way. It used a source, monochromator and a calibrated detector. The camera response was compared to the detector one. The measurements were made in the same ambient as well as geometric and lighting conditions (Zolin Neto 2012).

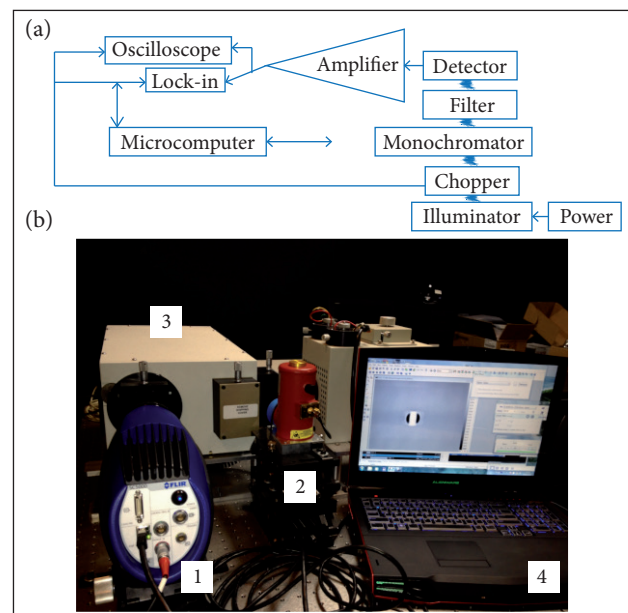


Figure 1. (a) Schematic diagram of the experimental arrangement; (b) Camera assembled for measurements.

RADIOMETRIC CHARACTERIZATION

The experimental arrangement (Fig. 2) was used to perform the radiometric characterization, where 1 represents the camera and 2, the blackbody. In this arrangement, in addition to the camera, it is also used a blackbody SR800 (CI Systems 2004). The camera was placed perpendicularly to the blackbody surface, at 1.55 m. This distance was chosen so the complete Schott's Contrast Transfer Function (CTF) could be obtained for the spatial characterization. For all measurements, the largest thermalization time was awaited. According to the camera manufacturer, this time is 2 h. An integration time of 1.6 ms was chosen, as recommended by FLIR® Systems, for temperatures between 10 and 55 °C. The sample rate was 60 Hz. For each established temperature in the blackbody, the data provided by the camera were the medium value of digital levels. For radiance and target temperature measurements, the surface emissivity was considered equal to 1 for the blackbody and 0.97 (aluminum) for the target.

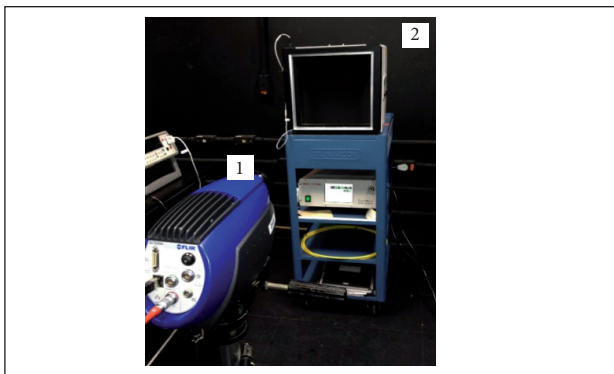


Figure 2. Experimental setup for radiometric characterization.

SPATIAL CHARACTERIZATION

For spatial characterization, 2 standard-based targets USAF 1951 (Applied Image Inc 2017) were machined. The target drawing, dimensioned in mm, is presented in Fig. 3. They were used as a mask for the blackbody (Fig. 4). The 2 targets/masks, one in aluminum and the other in steel, were produced by the Divisão de Suporte Tecnológico of the Instituto de Estudos Avançados (Fig. 5). The plates were square-shaped with 303.5 mm sides to be embedded in the extensive blackbody SR800 CI Systems, as a mask. The targets were sandblasted to increase the surface roughness, thereby reducing the specular reflection and increasing the Lambertian behavior of the electromagnetic waves reflected on the surface. The steel target

was also painted black, because, even after sandblasting, it showed some specular reflection.

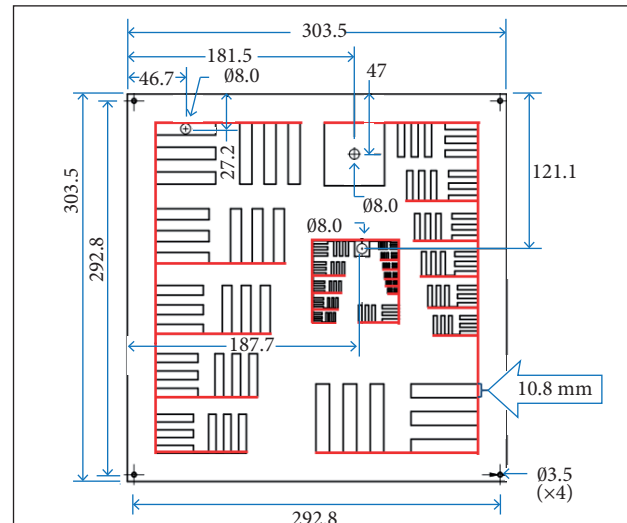


Figure 3. Mask fabrication drawing (dimensions in mm).

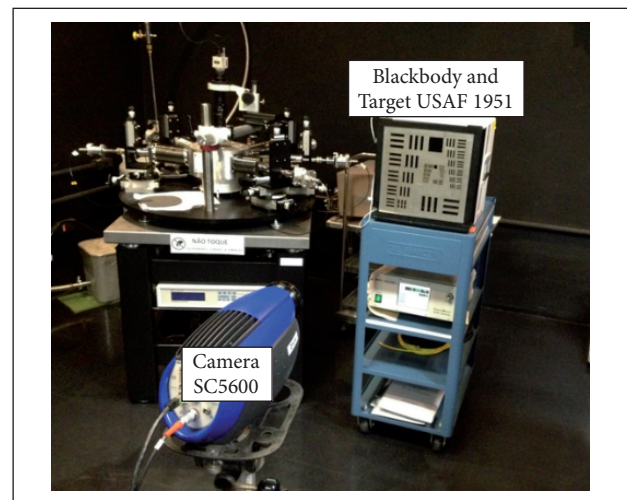


Figure 4. Spatial characterization arrangement with aluminum mask in front of the blackbody.

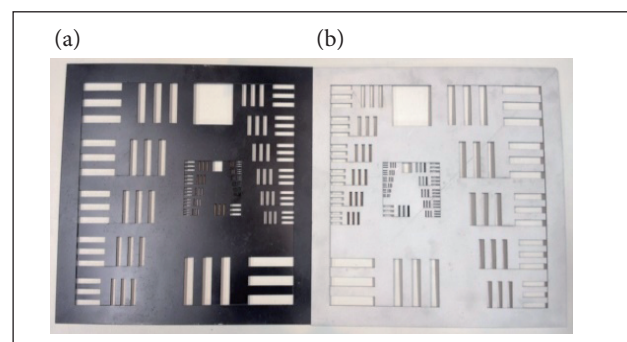


Figure 5. Steel (a) and aluminum (b) blackbody masks.

The blackbody was switched on, its temperature, adjusted to 40 °C, and the 1951 USAF metallic target was kept at room temperature (23.6 °C for steel and 22.4 °C for aluminum, measured by thermocouple). The absolute temperature difference between the blackbody and the target was enough to take the spatial characterization data, having the required radiometric contrast.

The data collection time was 1 s to guarantee there were no significant parameter changes along acquisition. Then, 60 samples of every image were obtained. The medium value of 60 values of each line (black or white) was obtained. A virtual mask was established to get the data and as many pixels as possible were evaluated for each pair of line pairs. For the highest spatial frequency, only 4 pixels were evaluated, as there was no room for more pixels. This virtual mask allowed the direct comparison between different temperature sets. Figure 6 presents the labels for data collection (Table 1) concerning the aluminum mask at room temperature and the blackbody at 40 °C.

For the target requirement fulfill the image, the target-to-camera distance of 1.55 m was chosen for the 27 mm focal length lens. Half and twice of this distance were also measured. The emissivity for the target used was 0.97. This is the value for the aluminum plate, as it has bigger area than the blackbody (emissivity equal to 1) on the image.

Data were analyzed and processed by Altair software (FLIR® Systems 2012). The medium values of the white lines (warmer, the blackbody) and the dark ones (colder, USAF 1951

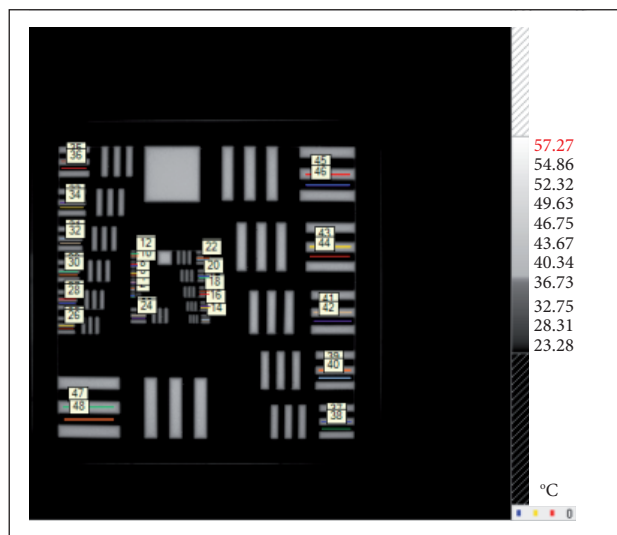


Figure 6. Data collect for the aluminum mask at room temperature and the blackbody at 40 °C.

Table 1. Data acquired from labels in Figure 6.

Label	Min (°C)	Max (°C)	Mean (°C)	Span (°C)	Standard deviation (°C)
31	37.94	38.22	38.12	0.28	0.07
32	23.12	23.33	23.26	0.20	0.05
33	37.90	38.16	38.09	0.26	0.06
34	23.08	23.30	23.19	0.22	0.06
35	38.02	38.20	38.14	0.18	0.04
36	23.03	23.21	23.12	0.17	0.04
37	37.90	38.23	38.15	0.33	0.07
38	22.88	23.10	22.99	0.22	0.05
39	38.16	38.41	38.30	0.25	0.05
40	22.83	23.03	22.94	0.21	0.05
41	38.28	38.52	38.43	0.24	0.05
42	22.80	23.00	22.90	0.15	0.04
43	38.42	38.57	38.50	0.21	0.04
44	22.82	23.00	22.92	0.18	0.04
45	38.41	38.60	38.50	0.19	0.04
46	22.82	23.03	22.92	0.21	0.04
47	38.36	38.55	38.47	0.19	0.04
48	22.65	22.84	22.75	0.19	0.04

target) were obtained. These values allowed to calculate the relative contrast, which is given by Eq. 1, normalized by the highest value.

$$Y = \frac{A - B}{A + B} \quad (1)$$

where: A is the average value in digital levels of the emitted radiation (through the bar area) by the blackbody; B is the average value in digital levels of the emitted radiation by the bar area from the Air Force Target 1951 (Fig. 7).

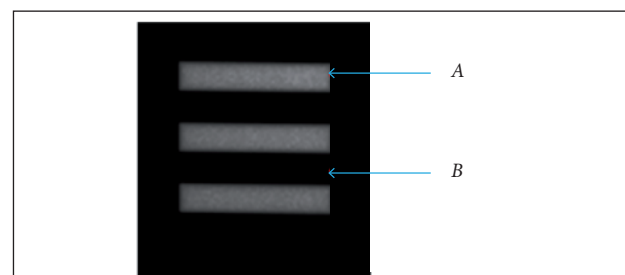


Figure 7. Area where the data were collected for each line pairs.

Having those values, the calculations of the CTF (Schott 2007) were held. Figure 8 shows the theoretical CTF preconized by Schott (2007), where the y -axis is the relative contrast described above.

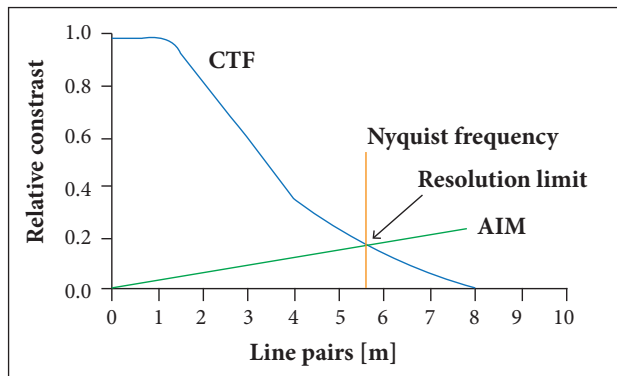


Figure 8. CTF, AIM and the resolution limit (Schott 2007).

NYQUIST FREQUENCY CALCULATION

The camera threshold resolution is limited by the Nyquist frequency, which is the inverse of 2 times the effective pixel size, and this (representation of the image) can be calculated using the total number of pixels of the target image and the actual size of the target. If the optical assembly is changed, a new value of the Nyquist frequency must be evaluated. The pixel size was calculated using the total number of pixels (353) in a row, corresponding to a line in the image target of 303.5 mm real size, for a distance of 1.55 mm from the camera. The value of the effective pixel size was $0.8598 \mu\text{m}$, and the correspondent Nyquist frequency was 582 cycles/m. This calculation was extended to the other distances and focal lengths (Table 2). Due to rounding on the figures of the effective pixel size, the values of the Nyquist frequency presented some differences. The line that connects the intersection of the CTF/Nyquist frequency curves to the graph origin indicates

Table 2. Nyquist frequency calculated for the 2 focal lengths and distances evaluated.

Focal length (mm)	Distance (m)	Effective pixel size (μm)	Nyquist frequency (cycles/m)
27	0.78	0.455	1,098
27	1.55	0.8598	582
27	3.12	1.718	291
54	1.55	0.4713	1,061
54	3.12	0.902	554

the lowest amount of modulation detected by a system (*i.e.*, other threshold). It is called Aerial Image Modulation (AIM) and it is the minimum required modulation to produce a response by the system (Almeida 2007). Any point below this curve must be disregarded (Fig. 8).

HOMEMADE BLACKBODY

In order to give more mobility to the experiments, a homemade blackbody was built, using spare parts of other systems. The main parts were:

- Digital Temperature Gauge and Controller, Robertshaw, LFS model, with K-type thermocouple (Chromel-Alumel), with measuring range of $70 - 1,200^\circ\text{C}$ (Fig. 9, item 1);
- A 3-L plastic tank (Fig. 9; item 2);
- A water pump, responsible for liquid circulation (Fig. 9; item 3);
- Serpentine (radiator) in a closed circuit with a fan for cooling;
- Resistance nickel-chromium (15 – 25% Cr, 19 – 80% Ni, with the remainder Fe) to heat the liquid;
- A copper sheet of $30.3 \times 30.3 \text{ cm}$ (painted with black ink on the front) with a copper coil welded on the back part;
- Thermal insulator at the back of the blackbody (Fig. 9; item 4); and
- Thermocouple (Fig. 9; item 5).

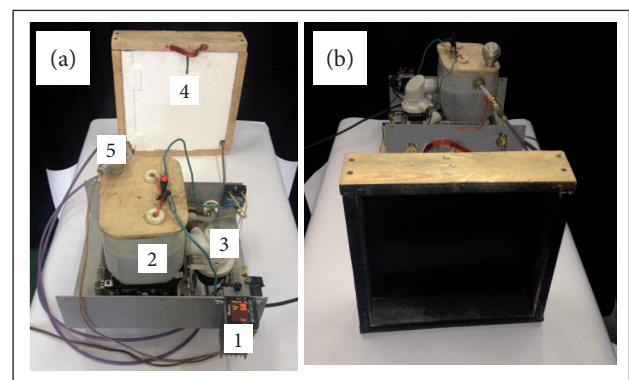


Figure 9. Main parts of the homemade blackbody.

RESULTS AND DISCUSSION

SPECTRAL CHARACTERIZATION

The voltage results from the reference detector, Wide Band Detector Judson Mercury Cadmium Telluride, were

taken as reference for camera data. Voltage measurements were performed for wavelengths from 2 to 7 μm at intervals of 50 nm. Three data sets were measured: no filter, filter number 2 and filter number 1 (Fig. 10a). The monochromator harmonics were subtracted, and the resulted plot is presented in Fig. 10b.

The camera replaced the Judson detector, and the same set of data was taken in digital levels to get the camera response curve — data obtained with shutter closed, no

filter and filter number 1 (Fig. 11a). The monochromator harmonics were subtracted, and the resulted plot is presented in Fig. 11b. The units were those available on the Altair Software.

The response curves provided by the manufacturer and the one obtained in this study can be compared (Fig. 12). The manufacturer's calibration process and data are not available, so the general curve behavior could be considered satisfactory.

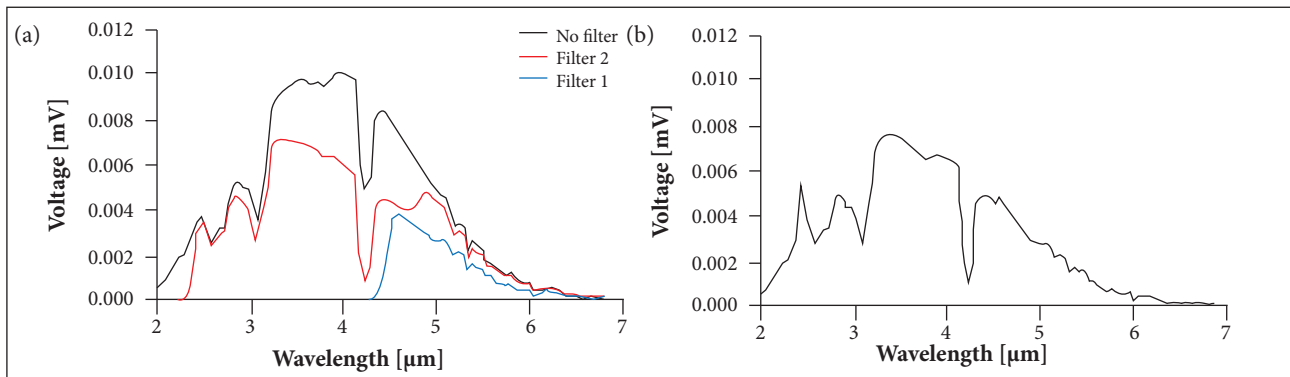


Figure 10. (a) Wide Band Detector Judson Mercury Cadmium Telluride; (b) Monochromator harmonics subtracted.

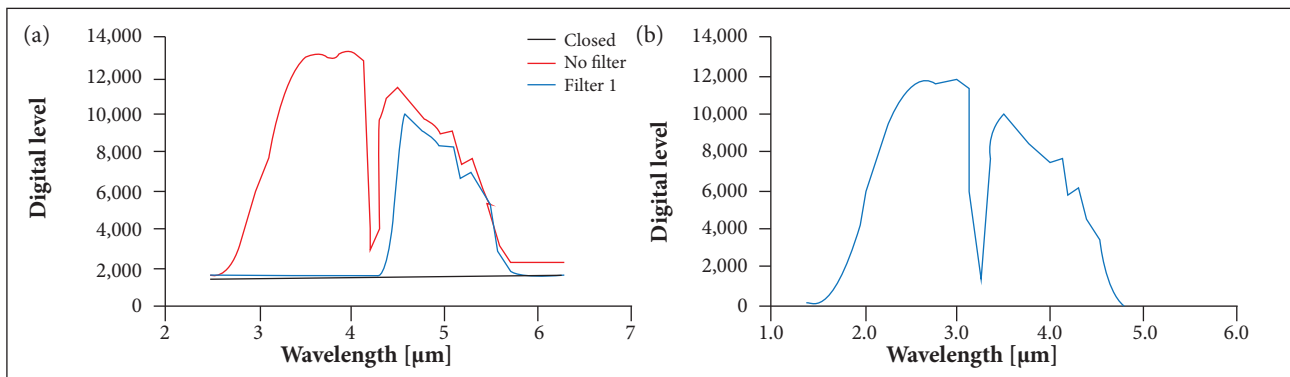


Figure 11. (a) Camera spectral characterization; (b) Monochromator harmonics subtracted.

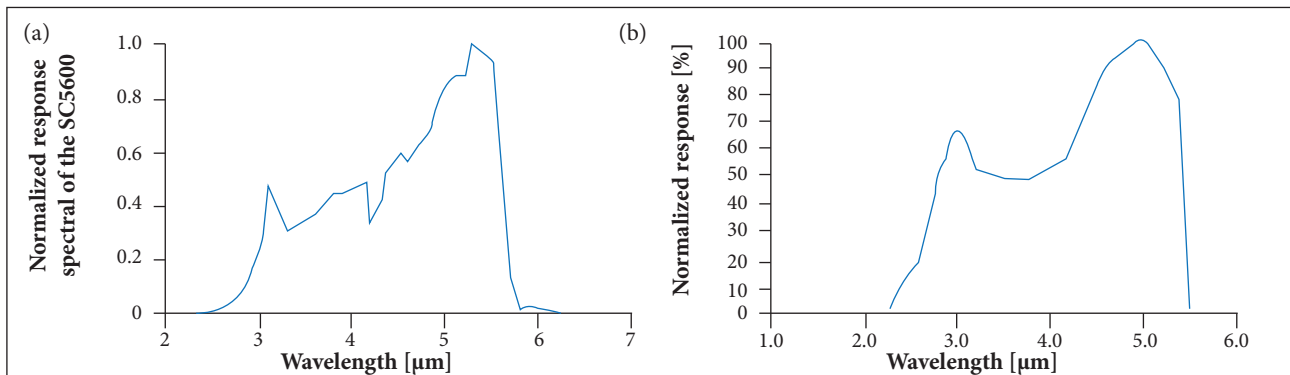


Figure 12. Response curves obtained in this study (a) and provided by the manufacturer (b).

RADIOMETRIC CHARACTERIZATION

For a set of blackbody temperatures, the temperature measured by the camera was registered (Fig. 13). Differences from $+0.25$ to -1.5 °C were found between the surface temperature set in the blackbody and the temperature measured by the SC5600 camera, using an emissivity of 0.97. These differences could be raised by factors that were not investigated as the value for the emissivity used may not be the real one, and the reflected radiation from surroundings may not have been considered correctly.

Another comparison was made between the calculated radiance and the one provided by the camera. The calculated radiance was obtained from the radiance emitted by the blackbody at the respective temperatures and the radiance reflected on it, coming from the laboratory (Fig. 14). A negligible difference was found. The calculated value of radiance does not include the radiance emitted by the environment air layer. Probably this was one of the factors that caused the difference between the calculated and measured radiances.

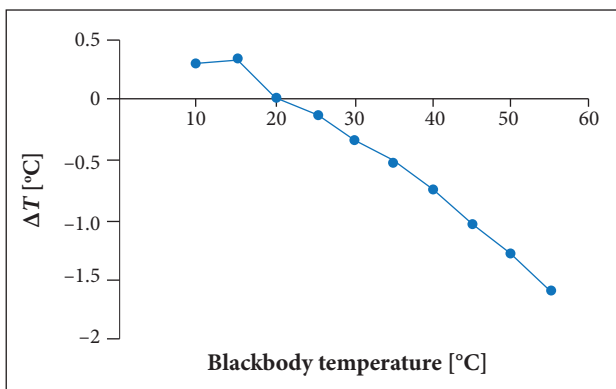


Figure 13. Temperature difference between what was set in the blackbody and measured by the camera.

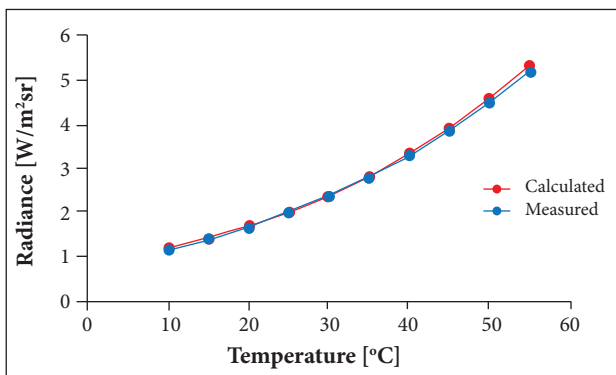


Figure 14. Calculated radiance and that provided by the camera.

The information provided by the camera is in digital levels. The conversion of the digital levels (DL) to radiance (L) is presented in Fig. 15. The linear dependence is clear. It also allows, for example, that a calibration curve for temperature be obtained.

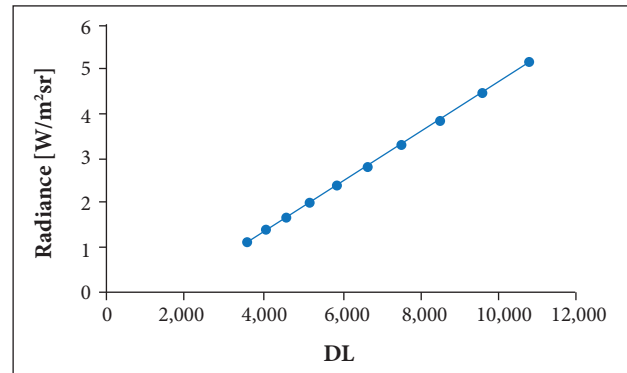


Figure 15. Conversion from DL to L.

SPATIAL CHARACTERIZATION

The camera was assembled with a 27-mm lens; an integration time of 1,600 us was set, and no filters were used; the steel target was at 23.6 °C (temperature measured by thermocouple) and the blackbody, at 40 °C. The distance between camera and blackbody was 1.55 m. It can be noted in the steel target that the 23rd and 24th elements on the 1951 USAF stayed below the sensor's resolution limit (Nyquist frequency); the 22nd element has been cut by the lack of contrast (AIM; Fig. 16). The 21st element was the last solved within the system's resolution limitation and with enough contrast. Each line of this element contains about 1.07 mm in width as the distance from the camera to the target was 1.55 m; each pixel in the sensor array provides 0.040° of

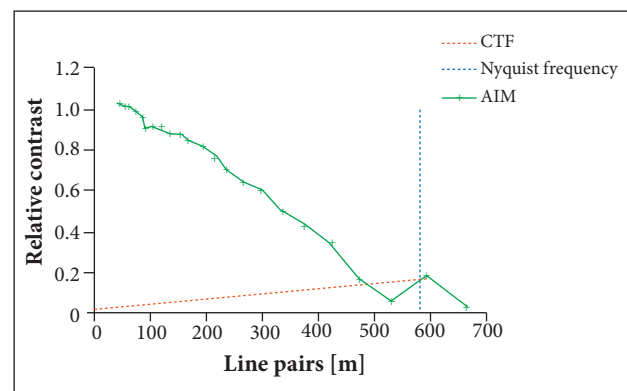


Figure 16. CTF results for steel mask at room temperature and blackbody set at 40 °C.

effective field of view. The results are summarized on Table 3, where n.a. means “not available”.

Table 3. Effective field of view for 2 sets of lenses and different camera blackbody distances.

Focal length (mm)	Distance (m)	Line pairs (cycles/m)	EIFOV (°)
27	0.78	1,098	n.a.
27	1.55	582	0.040
27	3.12	291	0.035
54	1.55	1,061	n.a.
54	3.12	554	0.017

EVALUATING THE UNCERTAINTY

Small conductance problems were found when using the steel target. Due to the target machining process, there was no physical contact between the ends of each tribar. The target was then replaced by one made of aluminum, whose conductivity showed best results (more uniformity).

The blackbody temperature was set between 10 and 55 °C, in steps of 5 °C, and all the CTFs showed similar profiles. The 23rd and 24th elements were below the sensor's resolution limit (the Nyquist frequency), and the 22nd one was disregarded due to lack of contrast, being below the uncertainty bar touching the AIM curve. The 21st element was the last solved within the system's resolution limitation and with enough contrast (Fig. 17). Each line of this element contains about 1.07 mm in width and, as the distance from the camera to the target was 1.55 m, each pixel in the sensor array provided a target effective field of view of 0.040°.

Smaller temperature differences between target and blackbody were analyzed. The smaller the difference, the worse the spatial resolution obtained. As an example, the aluminum target was set at 22.06 °C and the blackbody, at 21.90 °C. The temperature difference was of 0.16 °C, and the obtained result still presented a profile similar to that proposed by Schott (2007). Figure 18 shows that the 22nd – 20th elements were cut in the target due to lack of contrast (AIM); the 19th element could be also disregarded because the uncertainty bar is in the AIM curve, indicating to be in the contrast limit. The 18th element was the last solved within the system's resolution limitation and with sufficient contrast. Each line of this element contains approximately 1.5 mm wide as the distance from the camera to the target was 1.55 m; each pixel in the sensor array provided effective field of view of 0.055°.

For a 12 °C temperature difference, the 2 sets of lenses were tested at different distances. The idea was to evaluate the behavior of the CTF curves, having enough contrast condition, guaranteed by temperature difference. The distance taken for the previous data was 1.55 m for the 27-mm lens. Now it was evaluated the data for distances of 0.78 and 3.12 m (Fig. 19). As expected, the number of line pairs resolved was different. For the 54-mm lens, distances of 0.78 and 3.10 m were evaluated. Due to space limitations in the laboratory, the distance of 6.20 m could not be assessed.

Table 4 shows the resolution obtained for each available distance. It must be noticed that 2 effective instantaneous fields of view (EIFOVs) could not be determined (Table 3), as the smallest line of pairs was resolved far under the Nyquist frequency.

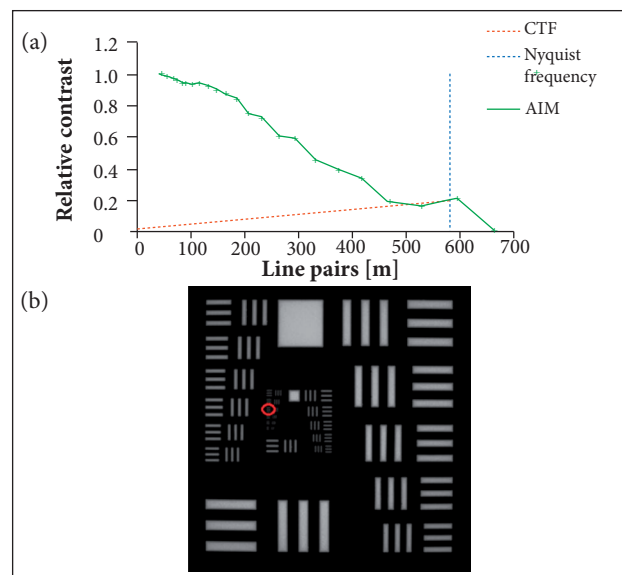


Figure 17. (a) CTF [aluminum mask, room temperature; blackbody, 40 °C]; (b) Last line pairs resolved.

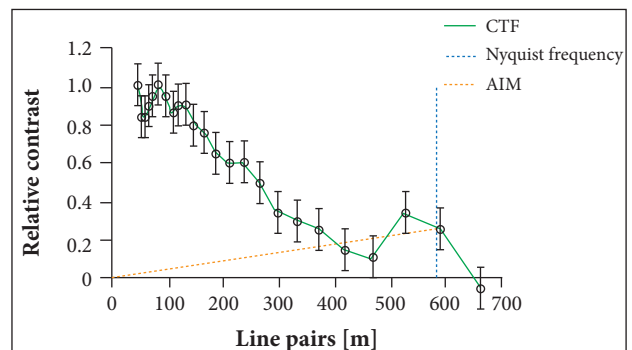
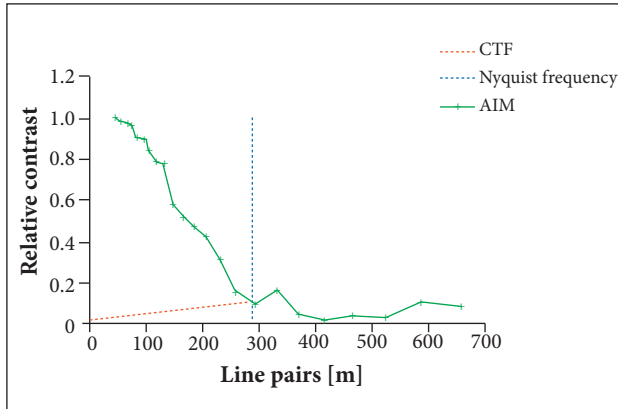


Figure 18. CTF results for very small temperature difference (0.12 °C) — blackbody at 22 °C.

Table 4. Results of direct comparison between the homemade and CI Systems blackbodies.

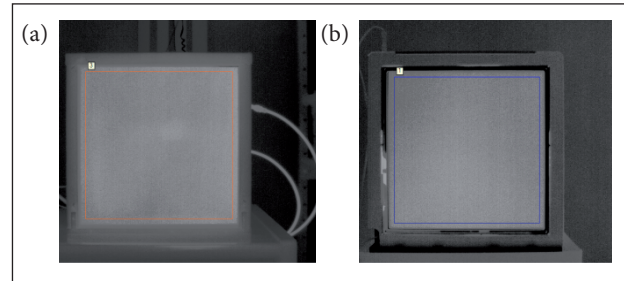
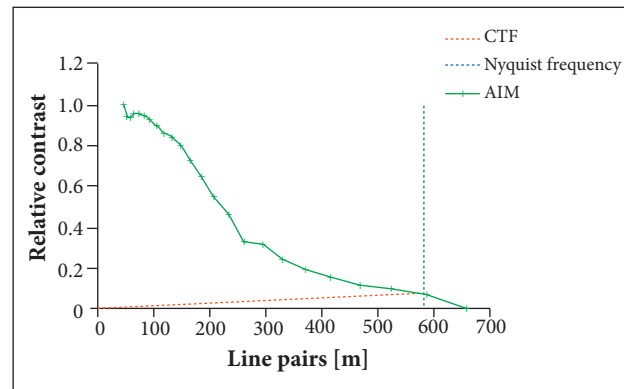
Blackbody	Minimum (°C)	Maximum (°C)	Mean (°C)	Span (°C)	Standard deviation	Emissivity	Surface
CI Systems	24.66	26.47	24.92	1.81	0.05	0.97	94,556
Homemade	24.36	24.79	24.58	0.43	0.05	0.97	94,554

**Figure 19.** CTF results for the 27-mm focal length lens, at 3.12 m, and blackbody at 35 °C.

OUTDOOR EXPERIMENT

The homemade blackbody non-uniformity was compared to the one of CI Systems. The blackbodies were set at the same temperature (with a measurable uncertainty) to compare results. The emissivity was set to 0.97 instead of 1, but this does not impede the comparison. The average temperature over the whole square (drawn over the blackbody surface and indicated by numbers 1 and 3 in Fig. 20) was compared. The standard deviation was the same, but the homemade one showed smaller span (Table 3).

In order to perform the experiment in non-controlled conditions, such as in laboratory, it was performed an outdoor experiment. The camera was assembled with a 27-mm lens, and the distance was 1.55 m. The CTF was obtained with the aluminum target at 28.14 °C and the blackbody, at 45.46 °C, both measured by the camera (Fig. 21). It presented a profile similar to that proposed by Schott (2007). It was observed that the 23rd and 24th target elements were below the 1951 USAF sensor's resolution limit (the Nyquist frequency). The 22nd element was the last solved within the system's resolution limitation and with sufficient contrast. Each line of the element contains approximately 0.95 mm width; as the distance from the camera to the target was 1.55 m, each pixel in the sensor array provides target field of 0.035°.

**Figure 20.** Measured areas on the homemade (a, in red) and CI Systems (b, in blue) blackbodies.**Figure 21.** CTF results using the 27-mm focus lens, in the outdoor experiment, with blackbody set at 45 °C.

CONCLUSION

This paper showed measurements for spectral, radiometric and spatial characterization to be applied on imaging systems operating in the thermal infrared. A SC5600 camera manufactured by FLIR® Systems was characterized.

The camera's spectral characterization was done by comparison with a calibrated system composed by thermal source, monochromator and a broadband reference detector. The results were similar to those provided by the manufacturer.

The radiometric characterization was performed using an extensive blackbody (CI Systems) for temperatures between 10 and 55 °C to verify the accuracy and obtain the calibration curves. Differences from +0.25 to -1.5 °C were found between

the surface temperature set in the blackbody and that obtained by the SC5600 camera, using an emissivity of 0.97. This is something unexpected as the manufacturer claims the camera sensitivity as 0.020 °C.

The spatial characterization was carried out using the same extensive blackbody (CI Systems) and 2 standard USAF 1951 machined targets, one made of steel and the other of aluminum, serving as masks for the blackbody. It was established a method to evaluate the EIFOV, which will allow to know the operational limits of the equipment.

Using recycled material, it was built a homemade extended blackbody for outdoor use. The results obtained, using the

homemade blackbody, were similar to those obtained at the laboratory.

AUTHOR'S CONTRIBUTION

Conceptualization, Damião AJ and Lima Filho GM; Methodology, Damião AJ, Almeida RCF, Castro RM, and Lima Filho GM; Investigation, Lima Filho GM, Castro RM, and Almeida RCF; Writing – Original Draft, Damião AJ and Lima Filho GM; Writing – Review & Editing, Damião AJ and Lima Filho GM.

REFERENCES

Almeida MH (2007) Desenvolvimento de um software para avaliação de desempenho do sistema óptico em equipamento para retinografia digital (Term paper). São Carlos: Universidade de São Paulo.

Applied Image Inc (2017) T-20 USAF 1951 Chart Standard Layout Product Specifications; [accessed 2017 Jul 6]. https://www.appliedimage.com/files/8sYYLo/USAF_1951_Test_Target_T-20_v1-Q4.pdf

Bower SM, Kou J, Saylor JR (2009) A method for the temperature calibration of an infrared camera using water as a radiative source. Review of Scientific Instruments 80, 095107. doi: 10.1063/1.3213075; [accessed 2017 Jul 6]. <http://cecas.clemson.edu/~jsaylor/paperPdfs/rsi.v80.n09.pdf>

CI Systems (2004) SR-800 extended area blackbody. Simi Valley; [accessed 2017 July 26]. <http://www.ci-systems.com/blackbodies>

FLIR® Systems (2012) Altair user manual. Hong Kong: FLIR® Systems.

FLIR® Systems (2017) SC5600-M. Large format infrared cameras for R&D and thermography applications; [accessed 2017 Jul 6].

http://www.sourcesecurity.com/datasheets/flir-systems-sc5600-cctv-camera/co-2752-ga/AU_SC5600-M_Leaflet_APAC.pdf

Johnson J (1958) Analysis of image forming systems. Proceedings of the Image Intensifier Symposium; Fort Belvoir, USA.

Lillesand TM, Kiefer RM (1994) Remote sensing and image interpretation. 3rd edition. New York: Wiley.

Pace PW, Sutherland J (2001) Detection, recognition, identification, and tracking of military vehicles using biomimetic intelligence. Proceedings of the 11th Automatic Target Recognition. Vol. 4379; Orlando, USA.

Schott J (2007) Remote sensing: the image chain approach. New York: Oxford University Press.

Schumaker DL (1996) The infrared and electro-optical systems handbook. Vol. 5. Ann Arbor: ERIM; Bellingham: SPIE.

Zolin Neto A (2012) Estudo de caracterização espectral de câmera termográfica (Term paper). São José dos Campos: Instituto Tecnológico de Aeronáutica.